APPLIED SCIENCES AND ENGINEERING

3D printing of highly stretchable hydrogel with diverse UV curable polymers

Qi Ge[1*†], Zhe Chen[2*], Jianxiang Cheng[1], Biao Zhang[3†], Yuan-Fang Zhang[4], Honggeng Li[4,5], Xiangnan He[1], Chao Yuan[4], Ji Liu[1], Shlomo Magdassi[6], Shaoxing Qu[2†]

Hydrogel-polymer hybrids have been widely used for various applications such as biomedical devices and flexible electronics. However, the current technologies constrain the geometries of hydrogel-polymer hybrid to laminates consisting of hydrogel with silicone rubbers. This greatly limits functionality and performance of hydrogel-polymer–based devices and machines. Here, we report a simple yet versatile multimaterial 3D printing approach to fabricate complex hybrid 3D structures consisting of highly stretchable and high–water content acrylamide-PEGDA (AP) hydrogels covalently bonded with diverse UV curable polymers. The hybrid structures are printed on a self-built DLP-based multimaterial 3D printer. We realize covalent bonding between AP hydrogel and other polymers through incomplete polymerization of AP hydrogel initiated by the water-soluble photoinitiator TPO nanoparticles. We demonstrate a few applications taking advantage of this approach. The proposed approach paves a new way to realize multifunctional soft devices and machines by bonding hydrogel with other polymers in 3D forms.

INTRODUCTION

Hydrogels, water-containing polymer networks, have found numerous applications in biomedicals (*1*–*3*), flexible electronics (*4*, *5*), and others (*6*, *7*). In many applications, hydrogels are combined with other polymers to form hybrid structures, which are used to protect, reinforce, or add new functionalities to hydrogel structures. Examples include elastomeric biomedical devices with hydrogel-based hydrophilic and lubricant skin (*8*–*10*), hydrogel-based flexible electronics with elastomeric antidehydration coating (*11*, *12*), hydrogel composites reinforced by elastomeric fibers (*13*, *14*), and others (*15*–*17*). Despite the recent rapid progresses, the polymers that hydrogels could be firmly bonded with are mainly restricted to silicone rubbers, and the geometries of hydrogel-polymer hybrids are mostly constrained to laminate structures (*8*, *9*, *11*, *12*), which greatly limit the functionality and performance of hydrogel-polymer–based devices and machines. Therefore, it is desired to develop an effective approach that fabricates hydrogel-polymer–based hybrid structures with high design freedom and rich material choice.

Three-dimensional (3D) printing that creates complex 3D objects in free forms has been broadly used to fabricate 3D hydrogel structures. Among all the 3D printing technologies, the extrusion-based direct ink writing (DIW) technology has been most widely adopted for 3D printing hydrogels (*18*–*20*). Different from DIW-based 3D printing, which forms 3D structures by directly extruding inks (*21*, *22*), digital light processing (DLP)–based 3D printing forms 3D structures through digitalized ultraviolet (UV) irradiation that triggers localized photopolymerization, turning liquid polymer resin to solid 3D structure, and therefore is an ideal technology to fabricate highly complex 3D structures with high resolution (*23*–*26*). Recently, Zhang and his co-workers (*27*) developed a highly stretchable and UV curable hydrogel, which is compatible with DLP-based 3D printing and enables the fabrication of high-resolution 3D hydrogel lattice structures with high water content [up to 90 weight % (wt %)] that can be stretched by up to 1300%. However, the capability of using DLP-based 3D printing to fabricate hybrid structures that consist of highly stretchable and high–water content hydrogels with other UV curable polymers has not yet been achieved. This is mainly because of the limited choice of highly efficient DLP-based multimaterial 3D printing system (*26*, *27*) and the lack of a universal approach that forms robust bonding between high-performance hydrogels with diverse UV curable polymers.

Here, we report a simple yet versatile multimaterial 3D printing approach that enables the fabrication of highly complex hybrid 3D structures consisting of highly stretchable and high–water content hydrogels that are covalently bonded with diverse water-insoluble UV curable polymers including elastomer, rigid polymer, acrylonitrile butadiene styrene (ABS)–like polymer, shape memory polymer (SMP), and other (meth)acrylate-based UV curable polymers. We demonstrate a number of applications taking advantage of this multimaterial 3D printing approach: hydrogel composites reinforced by horseshoe and lattice structures, 3D printed meniscus with spatially variable stiffness, 4D printing cardiovascular stent with drug delivery function as well as 3D printed ionic conductor, and strain sensor with antidehydration elastomeric layer. The proposed approach paves a new efficient way to fabricate soft devices and machines with greatly extended functionality and performance by bonding highly stretchable and high–water content hydrogel with other water-insoluble UV curable polymers, including elastomer, rigid polymer, ABS-like polymer, SMP, and other (meth)acrylate-based UV curable polymers in 3D forms.

[1]Department of Mechanical and Energy Engineering, Southern University of Science and Technology, Shenzhen 518055, China. [2]State Key Laboratory of Fluid Power and Mechatronic System, Key Laboratory of Soft Machines and Smart Devices of Zhejiang Province, Department of Engineering Mechanics, Zhejiang University, Hangzhou 310027, China. [3]Xi'an Institute of Flexible Electronics and Xi'an Key Laboratory of Biomedical Materials and Engineering, Northwestern Polytechnical University (NPU), Xi'an 710072, Shaanxi, China. [4]Digital Manufacturing and Design Center, Singapore University of Technology and Design, Singapore 487372, Singapore. [5]State Key Laboratory of Advanced Design and Manufacturing for Vehicle Body, Hunan University, Changsha 410082, China. [6]Casali Center for Applied Chemistry, Institute of Chemistry, The Center for Nanoscience and Nanotechnology, The Hebrew University of Jerusalem, Jerusalem 9190401, Israel.
*These authors contributed equally to this work.
†Corresponding author. Email: geq@sustech.edu.cn (Q.G.); iambzhang@nwpu.edu.cn (B.Z.); squ@zju.edu.cn (S.Q.)

RESULTS

Multimaterial 3D printing hydrogel with other polymers

As shown in Fig. 1A, we print the hydrogel-polymer heterogeneous structures on a self-built high-resolution, high-efficiency DLP-based multimaterial 3D printer (*24*, *25*). The system adopts "bottom-up" projection approach where digitalized UV light is irradiated from the UV projector, which is placed below the printing stage that moves vertically to control the layer thickness of each layer printing. Between the printing stage and UV projector, there is a polytetrafluoroethylene-coated glass plate that supports two to three polymer precursor solution puddles and moves horizontally to deliver a needed polymer precursor solution for the corresponding layer. The hydrogel used here is the highly stretchable and high–water content UV curable acrylamide-poly(ethylene glycol) diacrylate (PEGDA) (AP) hydrogel (*27*). The UV curable polymers are commercially available (meth)acrylate-based 3D printing polymers. Figure 1 (B and C) demonstrates the process of printing a diagonally symmetric Kelvin form where the half part is made of an elastomer (transparent) and the other half is made of AP hydrogel (yellow). When a layer of the elastomer part is being printed (Fig. 1B), the transparent elastomer precursor solution is placed below the printing stage, and the corresponding UV pattern is illuminated into the transparent elastomer precursor solution. As shown in Fig. 1C, when a layer of the hydrogel part is being printed, the yellow hydrogel precursor solution is positioned below the printing stage, and the corresponding UV pattern is irradiated into the hydrogel precursor solution. The air-jetting approach is applied to remove the precursor solution residuals on the printed part and minimize the material contamination during material exchange. Details about the DLP-based multimaterial 3D printing system can be found in note S1, fig. S1, and movie S1. As demonstrated in Fig. 1D, a diagonally symmetric Kelvin is finally printed by alternatively switching elastomer and hydrogel precursor solutions for each layer. As the strong covalent bonds are formed at the interfaces between the highly deformable AP hydrogel and elastomer, we can compress the printed multimaterial Kelvin form by 50% without finding any debonding between the two constituent materials (Fig. 1E and movie S2). To further demonstrate the versatility of this multimaterial 3D printing approach, we print a Kelvin foam where the three unit cells are printed with rigid polymer, AP hydrogel, and elastomer, respectively (Fig. 1F). Again, the hydrogel forms strong covalent bonds with the other two polymers, and we can stretch the hybrid Kelvin foam structure by large deformation without finding debonding between the unit cells printed with different materials (Fig. 1G and movie S3).

Materials and bonding mechanism

The illustrations in Fig. 2 further introduce the chemicals used to prepare this UV curable, highly stretchable, and high–water content

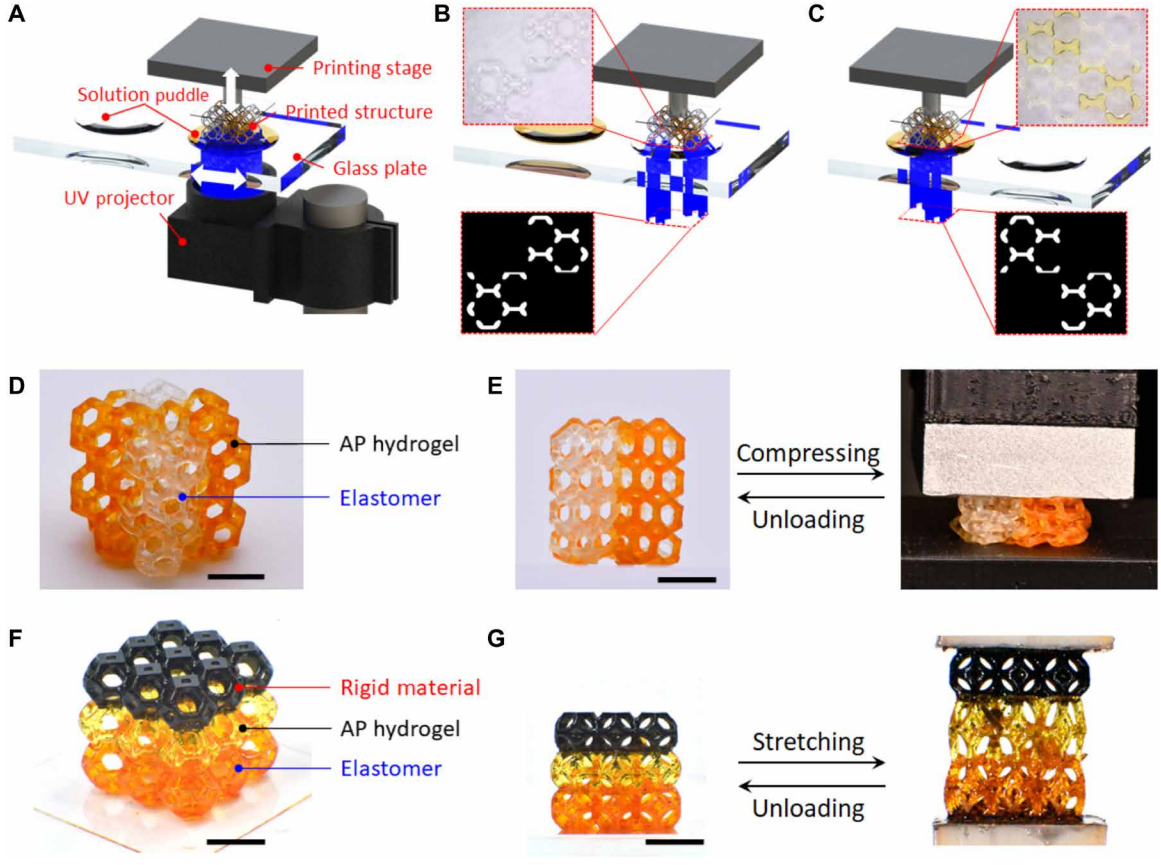

Fig. 1. Multimaterial 3D printing hydrogel with other polymers. (**A**) Illustration of the DLP-based multimaterial 3D printing apparatus. (**B** and **C**) Processes of printing elastomer and hydrogel structures, respectively. (**D**) Snapshot of a diagonally symmetric Kelvin form made of AP hydrogel and elastomer. (**E**) Demonstration of the high deformability of the printed diagonally symmetric Kelvin form. (**F**) Snapshot of a printed Kelvin foam consisting of rigid polymer, AP hydrogel, and elastomer. (**G**) Demonstration of the high stretchability of the printed multimaterial Kelvin foam. Scale bar, 5 mm. (Photo credit: Zhe Chen, Zhejiang University.)

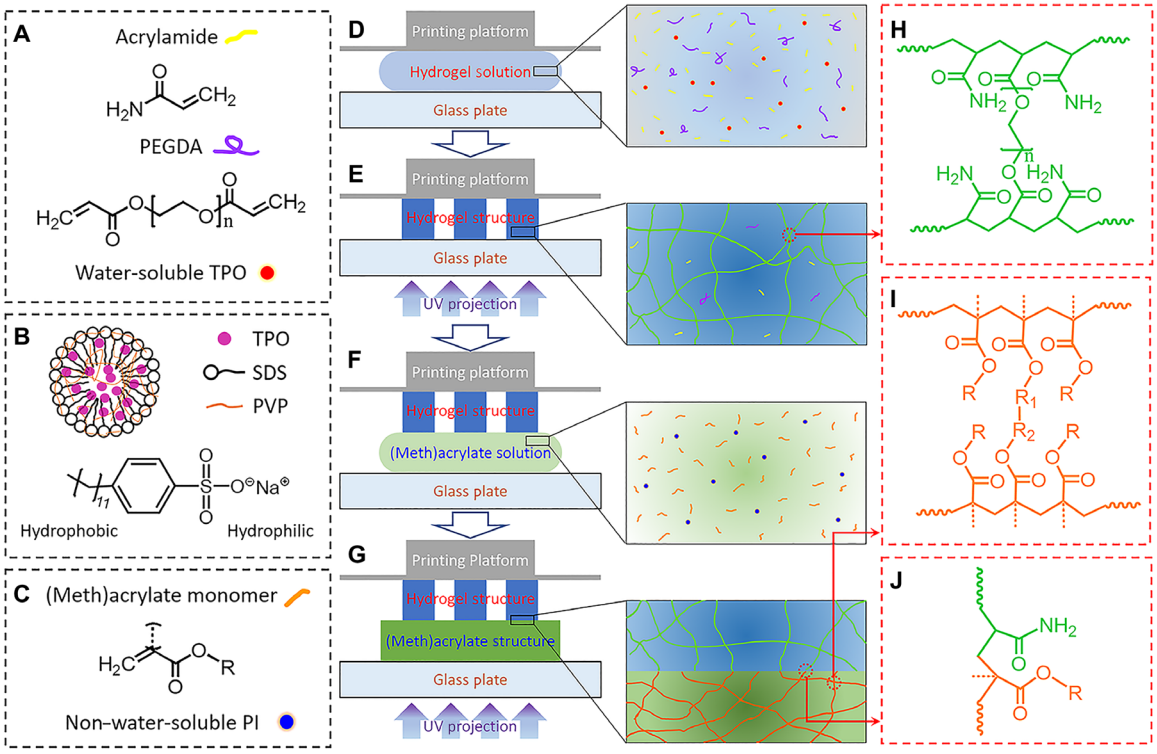

Fig. 2. Materials and bonding mechanism. (**A**) Chemicals used to prepare the AP hydrogel solution. (**B**) Illustration of the water-soluble TPO nanoparticle. PVP, polyvinylpyrrolidone. (**C**) Possible chemical structure of the (meth)acrylate-based polymer solution. PI, photoinitiator. (**D** to **G**) Schematics of the process of printing hydrogel-polymer multimaterial structure. (**H** to **J**) Chemical structures of cross-linked AP hydrogel, AP hydrogel–(meth)acrylate polymer interface, and cross-linked (meth)acrylate polymer, respectively. *R*, R_1, and R_2 are the possible middle chains in (meth)acrylate polymer.

AP hydrogel precursor solution and the mechanism that explains how the printed AP hydrogel could firmly bond with other (meth) acrylate-based UV curable polymers. As shown in Fig. 2A, we prepare the AP hydrogel precursor solution by mixing the acrylamide powders, PEGDA, and the self-prepared water-soluble photoinitiator 2,4,6-trimethylbenzoyl diphenylphosphine oxide (TPO) into water. Here, the PEGDA/acrylamide mixing ratio is 0.625 to 1.25 wt %, and the water content of the AP hydrogel is 70 to 80 wt % (details can be found in Materials and Methods). The mechanical behavior can be tuned by changing the PEGDA/acrylamide mixing ratio, the molecular weight of PEGDA, and the water content (*27*). Using water-soluble TPO as photoinitiator is the key to making the AP hydrogel precursor solution highly UV curable and 3D printable. To make the hydrophobic commercial TPO powders water soluble, we use the surfactant SDS that contains a hydrophilic head and a hydrophobic tail (Fig. 2B) to encapsulate TPO particles (*27*, *28*). In addition, polyvinylpyrrolidone is used as crystallization inhibitor. After freeze-drying the prepared oil-in-water microemulsions containing TPO, the highly water-soluble TPO nanoparticles are produced. Note that previous works report the approaches of using the commercial photoinitiator Irgacure 819 to prepare UV curable hydrogel precursor solutions (*29*–*32*). However, the water insolubility of Irgacure 819 requires users to dissolve it into organic solvent such as ethanol and dimethyl sulfoxide, which is only applicable to the hydrogels with relatively low stretchability and water content (*29*–*32*). To 3D print a hybrid structure consisting of AP hydrogel and other polymers, we choose a number of commercially available polymer precursor solutions (details can be found in Materials and Methods). Although the chemical details of these commercial polymer solutions are not given, they are (meth)acrylate-based monomers, cross-linkers, and oligomers with non–water-soluble photoinitiators (Fig. 2C).

Figure 2 (D to J) presents the multimaterial 3D printing process, the resulting chemical structures, and the proposed interface bonding mechanism between AP hydrogel and (meth)acrylate polymer. From Fig. 2 (D and E), the hydrogel precursor solution is solidified to a layer of hydrogel network structure upon a patterned UV projection. The photopolymerization cross-links acrylamide and PEGDA to form a chemically cross-linked network structure (Fig. 2H). Note that there is a small amount of unreacted acrylamide and PEGDA remaining in the polymerized hydrogel structure (Fig. 2E). From Fig. 2 (F and G), we further print a (meth)acrylate polymer layer onto the AP hydrogel layer by projecting a UV pattern into the (meth)acrylate polymer precursor solution, which leads to free radical photopolymerization (Fig. 2I). At the interface, the radicals within the (meth)acrylate polymer can also attack those unreacted monomers and oligomers within the AP hydrogel domain, resulting in the chemical bonding between the (meth)acrylate-based polymer layer and AP hydrogel layer (Fig. 2J and fig. S2).

To validate the mechanism that we propose to explain the interfacial bonding between AP hydrogel and (meth)acrylate polymer, we first carry out Fourier transform infrared (FTIR) spectroscopy to investigate the conversions of AP hydrogel polymerization initiated by different initiators. To compare conversion and kinetics of polymerization, we use another two initiators for comparison: (i) Irgacure 2959 (I2959), a commercial water-soluble photoinitiator

that has been widely used in DIW-based acrylamide hydrogel 3D printing (*18*), and (ii) ammonium persulphate (APS) as thermal initiator plus *N*,*N*,*N*′,*N*′-tetramethylethylenediamine (TEMED) as initiation accelerator, which have been widely used to synthesize bulk AP hydrogel samples (*33*). Figure 3A presents the FTIR spectrums of AP hydrogel before and after polymerization. The conversion can be calculated from the decay of the peak at 988 cm^{-1}, which is the out-of-plane bending mode of the $-CH_2-$ unit (methylene group), normalized to the C=O stretching peak (carbonyl group) at 1655 cm^{-1} as an internal standard. The conversions are ~100, ~90, and ~10% for the AP hydrogels initiated by APS-TEMED, TPO, and I2959, respectively. Details about sample preparation and FTIR tests can be found in Materials and Methods.

Since both TPO nanoparticle and I2959 are water-soluble photoinitiators, we further perform FTIR to investigate the photopolymerization kinetics of the AP hydrogel initiated by TPO and I2959, respectively. Details about the FTIR tests can be found in Materials and Methods and fig. S3. As shown in Fig. 3B, under the same UV curing condition, the AP hydrogel precursor solution initiated by TPO reaches 80% of conversion in 15 s, and its conversion is saturated at 90% after curing for 2 min. In comparison, the conversion of the AP hydrogel solution initiated by I2959 only reaches 10% after 2 min of UV curing. This is due to the extremely low photosensitivity of I2959 at 405 nm (molar extinction coefficient ε ~2 M^{-1} cm^{-1}), which is about 300 times lower than that of TPO (ε ~600 M^{-1} cm^{-1}) (*28*). On the basis of this, we conclude that AP hydrogel precursor solution with TPO is applicable to DLP-based 3D printing (the wavelength is usually 385 or 405 nm), which requires short UV exposure time (within 1 min) to cure a layer. AP hydrogel precursor solution with photoinitiator I2959 is only suitable to the DIW-based 3D printing, which allows users to print out 3D structures first and conduct a few hours of post-curing under even shorter wavelength UV irradiation to cross-link the hydrogel (*18*).

From Fig. 3A, we also find that APS-TEMED initiator converts almost 100% of acrylamide and PEGDA to the hydrogel covalent network; in comparison, the conversion of AP hydrogel with TPO is 90%. The difference in the conversions of polymerization is also reflected in the macroscopic mechanical behavior of the cross-linked hydrogels. Figure 3C presents the stress-stretch behavior of the AP hydrogel initiated by APS-TEMED and TPO, respectively. Details about the uniaxial tensile tests can be found in Materials and Methods. The one initiated by TPO exhibits lower stiffness and stretchability as the lower conversion of polymerization results in less cross-linking points and shorter linear chains. Although this relatively lower conversion of polymerization weakens the mechanical performance of the AP hydrogel, it is favorable for bonding the hydrogel with other UV curable (meth)acrylate polymers. To demonstrate that the TPO-initiated AP hydrogel with 90% polymerization conversion can form strong interfacial bonds with (meth) acrylate polymer, which the APS-TEMED–initiated AP hydrogel with 100% polymerization conversion cannot realize, we print a UV curable elastomer (*34*) onto a TPO-initiated AP hydrogel dogbone sample (Fig. 3D). Since the hydrogel and elastomer form strong chemical bonds, the hydrogel-elastomer hybrid sample can be stretched by five times without debonding. In contrast, the printed UV curable elastomer cannot form strong bonding with the APS-TEMED–initiated hydrogel, and the debonding occurs during stretching the hybrid sample (Fig. 3E). Taking this advantage of the TPO-initiated hydrogel, we further print the TPO-initiated AP hydrogel with other UV curable polymers. As shown in Fig. 3 (F to K), we stretch the hybrid dogbone samples where the AP hydrogel is arranged in series with Tango elastomer, Vero rigid polymer, Agilus elastomer, PEGDA, methacrylate SMP (*35*), and ABS-like polymer, respectively. Details about the UV curable polymers can be found in Materials and Methods, and uniaxial tensile testing results are presented in fig. S4. Since all the other UV curable polymers are stiffer than the AP hydrogel, most deformations appear on the hydrogel part. The energy needed to break the interfacial bonding between hydrogel and polymer is greater than the energy needed to break the hydrogel itself so that each hybrid sample fails when the hydrogel fractures rather than the debonding happens at the interface (Fig. 3, I to Q).

As illustrated in fig. S5A, we perform the 180° peeling tests to investigate the interfacial toughness between hydrogel and UV curable polymer (fig. S5B and movie S4). Notably, the force/width-displacement curves in fig. S5C indicate that the interfacial toughnesses for the AP hydrogel on the six different UV curable polymers in Fig. 3 (F to K) are similar to each other. This similarity can be explained by the images of the six fractured hydrogel-polymer hybrid samples during the peeling tests (fig. S5D). It can be seen that the AP hydrogel, instead of the hydrogel-polymer interface, undergoes a cohesive failure near the interface during the peeling tests, which leaves a residual layer of hydrogel on the polymer substrates (fig. S5D). The peeling tests confirm that the energy needed to break the hydrogel-polymer interface is greater the energy needed to break the hydrogel itself.

To further investigate the effect of the key printing parameter–UV curing time on the interfacial toughness, we also perform the peeling tests on the AP hydrogel–Tango elastomer hybrid samples where the AP hydrogels are cured with different time. As shown in fig. S6 (A and B), the interfacial toughness gradually increases from 11.3 to 19.7 J/m^2 (N/m) by increasing the UV curing from 10 s to 1 min, and it levels off when the UV exposure is longer than 1 min. The increase in the measured interfacial toughness is mainly due the increase in the fracture toughness of the pure AP hydrogel sample by increasing the UV curing from 10 s to 1 min (fig. S6C) as more monomers and cross-linkers are cross-linked. However, the variation in UV curing time does not affect the facture mode. As shown in fig. S6 (D to I), all the hydrogel-elastomer hybrid samples facture on the hydrogel side, and all fractures are cohesive even for the hybrid sample where the hydrogel is only cured for 10 s. In addition, we also perform the peeling test to investigate the interfacial bonding between the Tango elastomer and AP hydrogel initiated by photoinitiator I2959, which is cured in an oxygen-free environment under 254-nm-wavelength UV curing for 40 min. Figure S7 shows that the I2959-initiated AP hydrogel also undergoes cohesive failure, indicating that the proposed interfacial bonding mechanism also works for the I2959-initiated AP hydrogel, which could be used to print AP hydrogel with other polymers through DIW-based 3D printing.

3D printed rigid polymer–reinforced hydrogel composites

The ability of bonding with other UV curable polymers makes the TPO-initiated highly stretchable and high–water content AP hydrogel suitable for DLP-based multimaterial 3D printing. Using this ability, we can quickly and easily fabricate rigid polymer–reinforced hydrogel composites with superior mechanical performance and

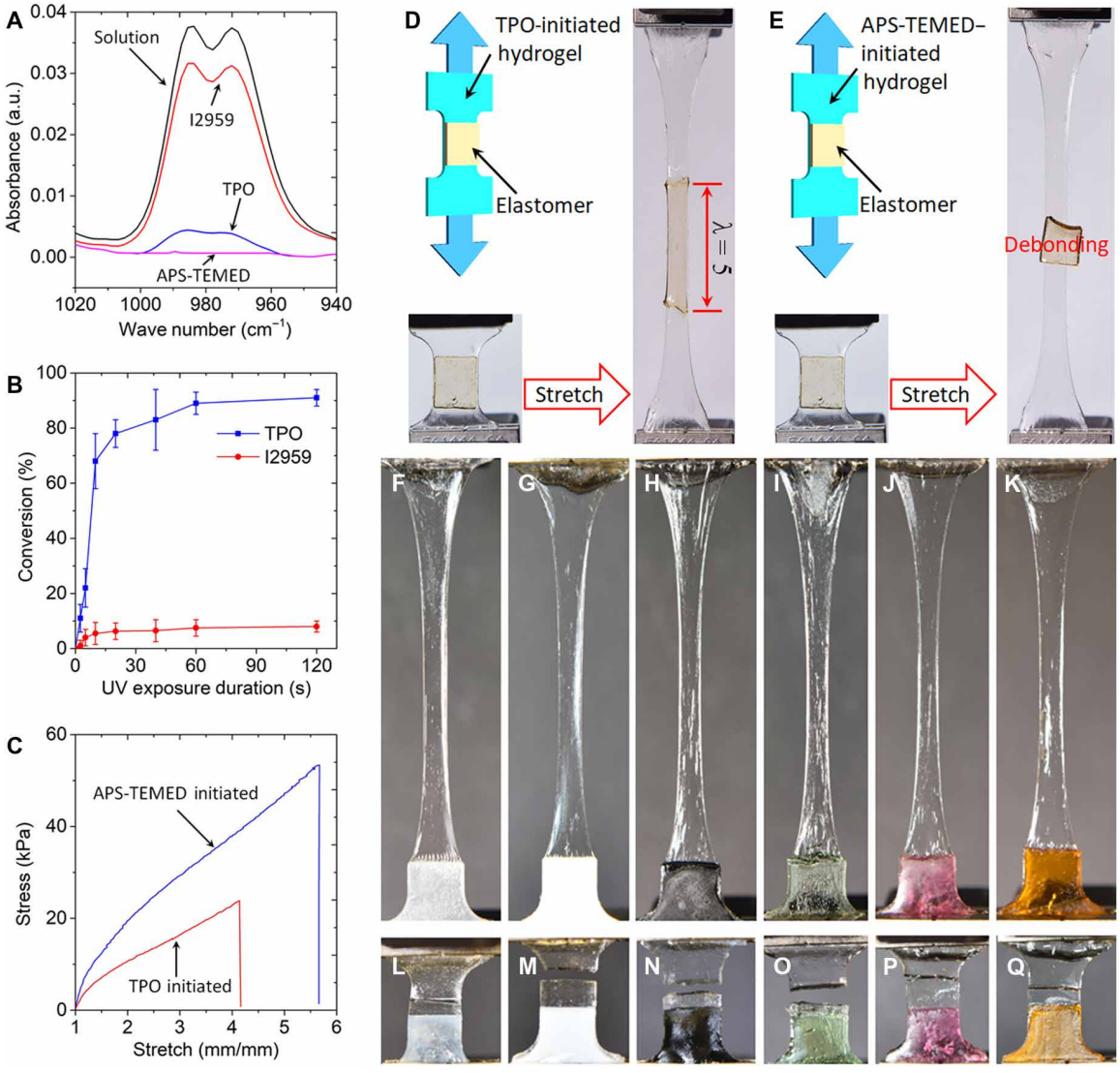

Fig. 3. Comparisons on polymerization conversion and bonding capability. (**A**) FTIR spectrums of AP hydrogels initiated by water-soluble TPO, I2959, and APS-TEMED, respectively. a.u., arbitrary units. (**B**) Comparison on photopolymerization kinetics of AP hydrogels initiated by TPO and I2959, respectively. (**C**) Comparison on the stress-stretch behavior of AP hydrogels initiated by TPO and APS-TEMED, respectively. (**D** and **E**) Demonstrations of bonding a UV curable elastomer to water-soluble TPO- and APS-TEMED–initiated hydrogel, respectively. (**F** and **G**) Uniaxial tensile tests of the dogbone samples printed with half AP hydrogel and half Tango elastomer (F), Vero rigid polymer (G), Agilus elastomer (**H**), PEGDA (**I**), methacrylate-based SMP (**J**), ABS-like polymer (**K**), respectively. (**I** to **Q**) Snapshots of the corresponding raptured samples. (Photo credit: Zhe Chen, Zhejiang University.)

design flexibility, which have not yet been achieved (see table S1) (*13*, *36*–*38*). As shown in Fig. 4A, we print a hydrogel composite reinforced by the Vero rigid polymer where the horseshoe structure design of rigid polymer is adopted to accommodate the large stretchability of the hydrogel (*39*). The strong bonding between the hydrogel and rigid polymer enables the large deformation of the composite without debonding (Fig. 4B). The multimaterial 3D printing of hydrogel–rigid polymer composite increases the material stiffness by ~30 times with a reasonably good stretchability (Fig. 4C). The mechanical performance of the horseshoe microstructure–reinforced hydrogel composite can be further tuned by adjusting the geometries of horseshoe unit cell (*40*) or assembling the horseshoe unit cells in different 2D topologies (*41*). Moreover, the high design and manufacturing flexibility of 3D printing allows us to fabricate hydrogel composite with gradient stiffness by tuning the microarchitecture of the reinforcing rigid structure. As shown in Fig. 4D, we print a hydrogel composite cube reinforced by a rigid lattice structure with gradually decreased stiffness from bottom to top by reducing the diameter of truss rod from 0.5 to 0.2 mm (Fig. 4E). We perform uniaxial compressive tests (see details in Materials and Methods) to characterize the stiffness for the hydrogel composites reinforced by the lattice structure with different rod diameters (fig. S8), and the tests reveal that the stiffness of a pure hydrogel (~10 kPa) can be reinforced to 0.6 to 5 MPa by tuning the rod diameter of the lattice structure from 0.2 to 0.5 mm (Fig. 4F). Hydrogel is a biocompatible material that has been widely

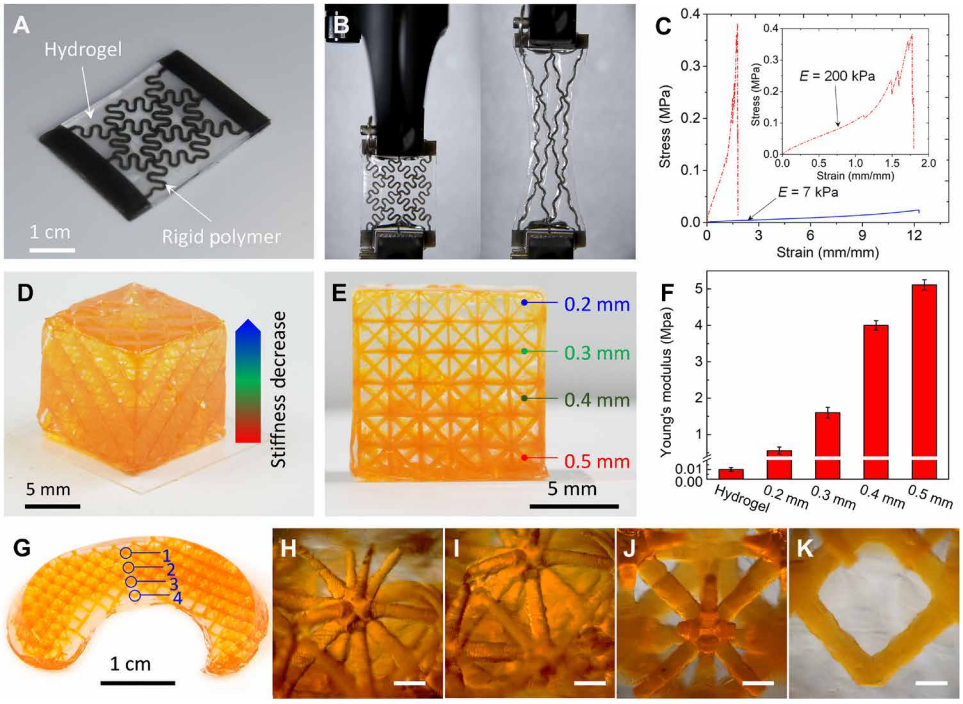

Fig. 4. 3D printed rigid polymer–reinforced hydrogel composites. (**A** to **C**) Hydrogel composite reinforced by horseshoe rigid polymer structure. (A) Isotropic picture of a printed composite. (B) Snapshots of the composite before uniaxial tensile test (left) and after stretched by 175% (right). (C) Comparison of the stress-strain behavior between pure hydrogel and composite. (**D** to **F**) Hydrogel composite reinforced by rigid polymer lattice structure. (D) Isotropic picture of a printed composite cube with gradient stiffness. (E) Front view of the printed composite cube where the diameter of truss rod decreases from 0.5 to 0.2 mm. (F) Measured compressive modulus for pure hydrogel and rigid polymer lattice structure–reinforced hydrogel with different rod diameters. (**G**) Snapshot of a printed meniscus made of hydrogel reinforced by rigid lattice structure. (**H** to **K**) The corresponding microscopic images of the microstructures at locations 1 to 4 within the printed meniscus (scale bars, 500 μm). (Photo credit: Zhe Chen, Zhejiang University.)

applied to various biomedical applications. However, in many applications, the stiffness mismatch between hydrogel and human tissue becomes a great challenge (*40*). The multimaterial 3D printing of rigid polymer reinforced hydrogel provides a promising solution to address this. To demonstrate this concept, we print a meniscus consisting of AP hydrogel reinforced by Vero rigid polymer (Fig. 4G). The manufacturing freedom of 3D printing enables us to tune local mechanical property within the meniscus depending on the anisotropic nature of meniscus. Figure 4 (H to K) presents the microstructures at locations 1 to 4 within the printed meniscus. By tuning the rod diameter from 0.2 to 0.5 mm, we can increase the local stiffness from 0.6 to 5 MPa. This capability of tuning local mechanical property by varying the rigid microstructures will greatly enhance the functionality and performance of 3D printed biological materials and tissues.

Printed SMP stent with drug releasing function

As illustrated in Fig. 5A, SMP is an ideal 4D printing material (*32*) for 3D printing shape memorable cardiovascular stent to expand the blood vessel with stenosis. By taking advantage of multimaterial 3D printing, we can impart the drug releasing function into a cardiovascular SMP stent by integrating hydrogel into the SMP stent. Figure 5B presents the design of the multimaterial stent where the major stent structure is printed with SMP, and hydrogel skins (thickness: 200 μm) are embedded into the SMP rods (Fig. 5C). As illustrated in Fig. 5D, since the stent has the shape memory effect, it can be squeezed into a compacted shape at the programming temperature, and the compacted shape can be fixed after cooling to a lower temperature, which is lower than the glass transition temperature (T_g) of the SMP; the compacted stent recovers to its original shape after heating back the programming temperature. As shown in Fig. 5E, we modify the commercial UV polymer VeroClear to reduce its T_g to 30°C (for details, see Materials and Methods) so that we can program the SMP-hydrogel stent at 37°C and the compacted shape can be fixed at 20°C (the shape memory cyclic test is presented in fig. S9). As presented in Fig. 5F, we use the self-built multimaterial DLP printer to fabricate the SMP-hydrogel stent. We load red dye as "drugs" into the AP hydrogel precursor solution (red dye concentration: 2.5 mM/liter). The stent can be fixed to the compacted shape due to the shape memory effect (Fig. 5G). Moreover, as shown in Fig. 5H, the fabrication flexibility of multimaterial 3D printing allows us to vary the size of the SMP-hydrogel stents to adapt the size variation of different blood vessels.

Figure 5I presents an example to demonstrate both shape memory and drug releasing functions of the printed SMP-hydrogel stent. We fabricate a polydimethylsiloxane (PDMS) tube whose diameter varies to a smaller value in the middle to simulate the vessel stenosis. The tube is filled with 37°C phosphate-buffered saline (PBS) solution to mimic the body environment. The expansion of the stent is observed 2 min after it is inserted into the PDMS tube (movie S5), and the stent fully expands after 1 hour, which is consistent with the shape memory cyclic test in fig. S9. After we insert the stent

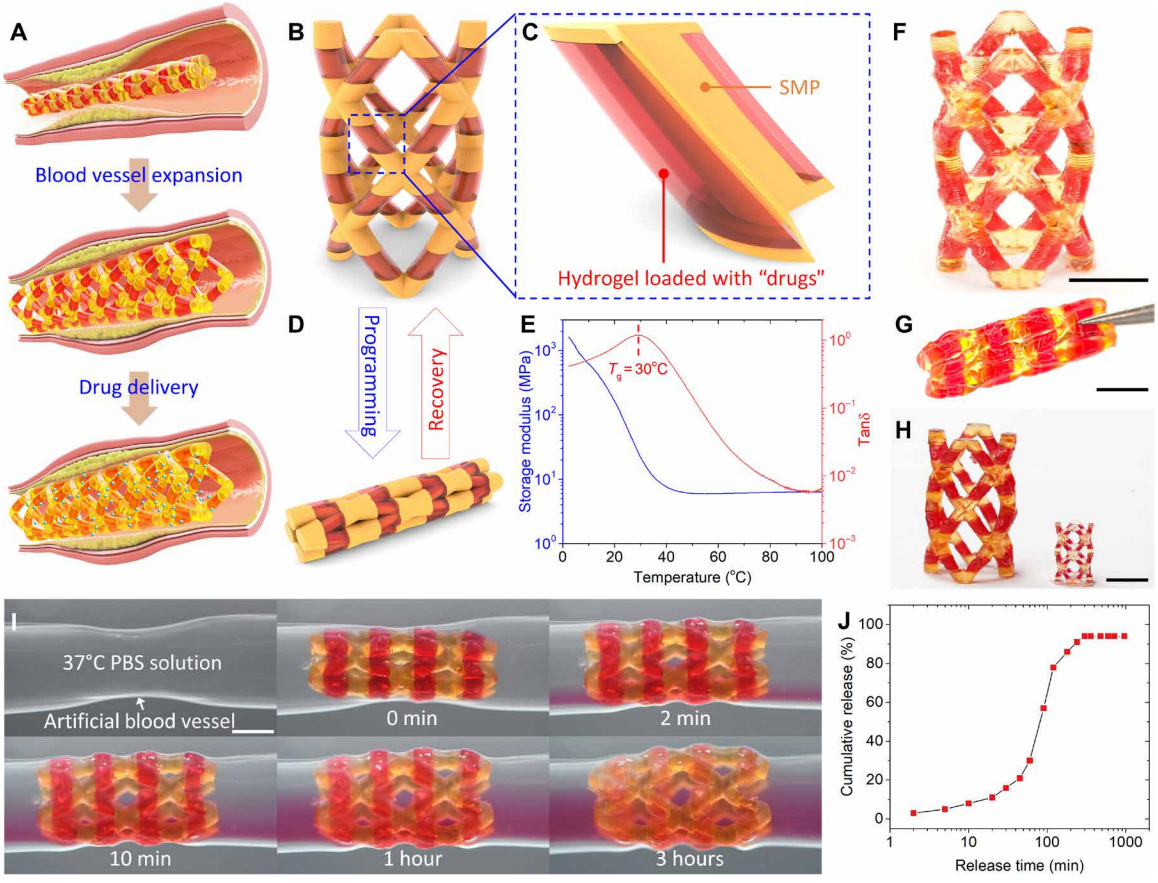

Fig. 5. Printed SMP stent with drug releasing function. (**A**) Illustration of the blood vessel expansion and drug releasing functions of the printed SMP-hydrogel stent. (**B**) Overall design of the SMP-hydrogel stent. (**C**) Detailed design shows that the SMP rod is surrounded the hydrogel skin loaded with drugs. (**D**) Illustration of the SMP-hydrogel programmed to a compacted shape. (**E**) DMA result indicates that the T_g of the SMP used to print the stent is 30°C. (**F** to **H**) Snapshots of printed SMP-hydrogel stents. (F) As-printed SMP-hydrogel stent. (G) SMP-hydrogel stent in programmed compacted shape. (H) SMP-hydrogel stents with different sizes. (**I**) Example to demonstrate both shape memory and drug releasing functions. (**J**) Quantified drug releasing process. Scale bar, 5 mm. (Photo credit: Jianxiang Cheng, Southern University of Science and Technology.)

to the tube, the hydrogel starts to release the drugs into the aqueous environment, and the drug releasing process is observed by seeing the color change of the PBS solution. We further quantify the drug releasing process through UV-visible spectrum (note S10 and fig. S10). In Fig. 5J, the hydrogel releases 3, 16, and 30% of the total drugs within 2 min, 30 min, and 1 hour, respectively. After 3 hours, the cumulative release saturates at about 90%. As shown in fig. S11, after being placed in the 37°C PBS solution for 24 hours, the SMP-hydrogel SMP releases the drugs completely, and the SMP rod can be clearly seen through transparent swollen hydrogel skin. On the basis of the real application requirements, the rate of drug release can be further controlled by tuning the size ratio between the hydrogel mesh and drug particles (*42*), adopting the hydrogel-particle dual-release mechanism (*43*), using environmental responsive hydrogels that release drug in response to the change in pH or temperature (*44*).

Printed flexible electronic devices with ionic conductive hydrogel

The ionic conductivity is another promising property, which allows hydrogels to be used in the applications of flexible electronics (*5*, *30*). However, the traditional manufacturing greatly limits the geometrical complexity of hydrogel structures so that the reliability and functionality of manufactured flexible electronics. The capability of 3D printing hydrogel with elastomer offers a promising solution to address this challenge. As shown in fig. S12, we print a 3D ionic conductive hydrogel lattice structure with elastomer protective skin, which protects the structure from water evaporation. Moreover, we can use the capability of 3D printing hydrogel with elastomer to fabricate more complex conductive hydrogel–integrated devices and machines. To demonstrate this, we print a soft pneumatic actuator (SPA) where a conductive hydrogel–based strain sensor is integrated. Figure 6A presents the schematic design of the actuator, and Fig. 6B shows the printed SPA with the hydrogel sensing circuit highlighted in pink color. In comparison with previously reported approaches (see table S2) (*45*–*48*), we only need one single step to fabricate the SPA with strain sensor due to the strong interfacial bonding between the UV curable hydrogel and elastomer. To achieve the relation between resistance and deformation, we print the hydrogel sensing circuit on an elastomer substrate. We stretch the substrate along the length direction to characterize the relation between resistance and tension and stretch the substrate along the

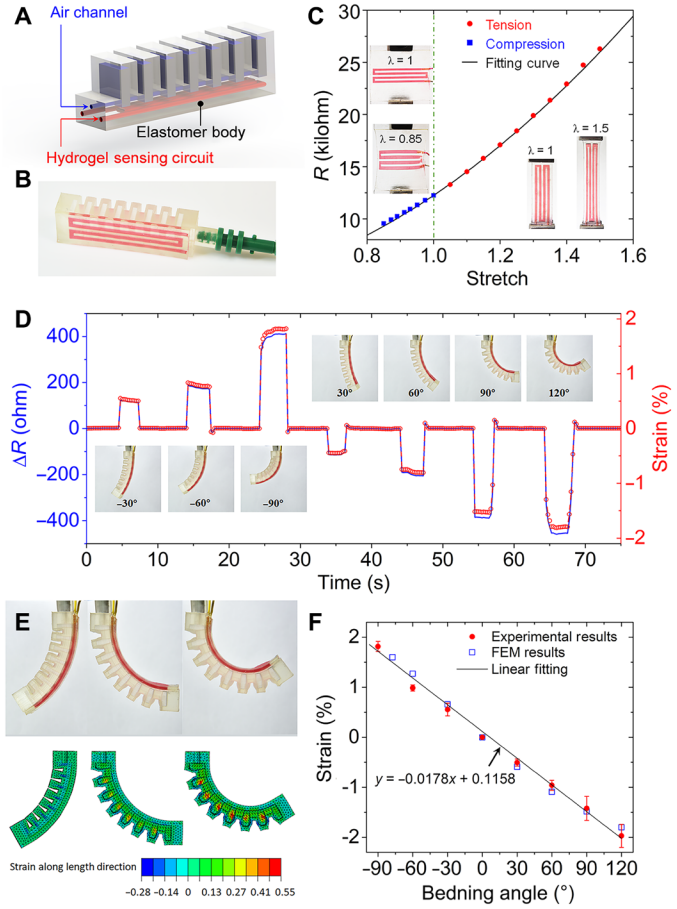

Fig. 6. Printed soft pneumatic actuator with hydrogel strain sensor. (**A**) Schematic illustration of the SPA design. (**B**) Image of a printed SPA with hydrogel strain highlighted in pink color. (**C**) Experiments to investigate the resistance-stretch relation. (**D**) Bending sensor characterization. (**E**) Comparison between experiments and FEA simulations. (**F**) Relation between bending angle and measured strain on the sensor. (Photo credit: Zhe Chen, Zhejiang University.)

width direction to capture the relation between resistance and compression (Fig. 6C). We further derive an equation to describe the relation between resistance and stretch: $R = a\lambda^2 + b\lambda^{-1}$ with $a + b = R_0$ (initial resistance R_0 = 12,249 ohms and fitting parameter a = 11,250 ohms). Details about the derivation can be found in note S9 and fig. S13. Figure 6C shows that the derived equation is able to nicely capture the nonlinear resistance-deformation behavior. Using the derived equation, we can transform the measured resistance variation to the strain on the SPA under bending. As shown in Fig. 6D, when a negative pressure is applied, the bending angle is defined as negative, and the measured strain is positive since the layer where the hydrogel sensor locates is being stretched. The measured strain becomes negative when we apply a positive pressure, which leads to positive bending of the SPA where the hydrogel sensor is being compressed. Note that compared with the previously reported SPA with strain sensor (see table S2) (*45*–*48*), we are the first that can measure the compressive strain on the SPA so that the strain sensor developed here can measure the actuations with both positive and negative bending. We further conduct finite element analysis (FEA) (see details in Materials and Methods) to simulate the bending of the SPA and achieve the relation between the bending angle and the strain on the position where the sensor is placed. As shown in Fig. 6 (E and F), the FEA simulations agree with the experiments well, and the bending angle and the strain follow a liner relation. On the basis of this relation between bending angle and strain and the relation between resistance variation and strain, the SPA can sense its instantaneous bending during actuation (*49*, *50*).

DISCUSSION

We developed a simple yet versatile multimaterial 3D printing approach that enables the fabrication of highly complex hybrid 3D structures consisting of high–water content, highly stretchable hydrogels that are covalently bonded with various other UV curable polymers. We used a self-built DLP-based multimaterial 3D printer to fabricate hydrogel-polymer hybrid 3D structures. We enabled the UV curability of the AP hydrogel using an amphipathic surfactant (SDS) to convert the hydrophobic photoinitiator TPO powders into highly water-soluble TPO nanoparticles. During multimaterial 3D printing, the unreacted monomers and cross-linkers remaining in the TPO-initiated hydrogel form covalent bonds at the hydrogel-polymer interface. We proved the hypothesis about the hydrogel-polymer interface bonding by FTIR and mechanical tests. We demonstrated a number of applications taking advantage of this multimaterial 3D printing approach: hydrogel composites reinforced by horseshoe and lattice structures, 3D printed meniscus with spatially variable stiffness, 4D printing cardiovascular stent with drug releasing function as well as 3D printed ionic conductor and strain sensor with an antidehydration elastomeric layer.

MATERIALS AND METHODS

Preparation of AP hydrogel solution

The AP hydrogel solution was prepared by mixing the AP mixture with self-developed highly water-soluble, high-efficiency photoinitiator, TPO nanoparticles (*27*, *28*). The water content of the solution is 70 to 80%. We choose acrylamide as monomer to form highly stretchable hydrogels and use PEGDA (M_w = 700) as cross-linker to tune the cross-linking density and the mechanical performance of the hydrogel system. The mixing ratio of PEGDA/acrylamide is 0.625:100. The mixing ratio between TPO and AP is 5%. All the chemicals were purchased from Sigma-Aldrich (St. Louis, MO, USA) and used as received.

UV curable (meth)acrylate polymer solutions

All the UV curable (meth)acrylate polymer solutions were directly purchased from 3D printing companies or synthesized by using commercially available chemicals. Tango elastomer, Vero rigid polymer, and Agilus elastomer were purchased from Stratasys Ltd. (Eden Prairie, MN, USA), and ABS-like polymer was obtained from Kudo3D Ltd. (Dublin, CA, USA). PEGDA solution was prepared by mixing PEGDA (M_w = 700) with photoinitiator TPO. The mixing ratio of TPO/PEGDA is 2:98. The methacrylate-based SMP solution was prepared by mixing benzyl methacrylate (BMA) with poly(ethylene glycol) dimethacrylate (PEGDMA; M_w = 550). The mixing ratio of BMA/PEGDMA is 70:30. TPO as photoinitiator was mixed into BMA-PEGDMA solution at the concentration of 5% by weight. In both PEGDA and BMA-PEGDMA solutions, Sudan I as photo absorber was added at a concentration of 0.05% by weight. All the chemicals used to prepare PEGDA and BMA-PEGDMA solutions

were purchased from Sigma-Aldrich (St. Louis, MO, USA) and used as received.

Multimaterial 3D printing hydrogel with other polymers

We printed all the hydrogel-polymer heterogeneous 3D structures on a self-built DLP-based multimaterial 3D printing system. Details about the multimaterial 3D printer and printing process can be found in note S1 and fig. S1. The estimated printing time of structures shown in Figs. 1 (D and F), 4 (A, D, and G), 5F, and 6A are presented in note S13 and tables S3 to S9.

FTIR characterizations

To compare the conversions of polymerization (Fig. 3A), we prepared the hydrogel consisting of 80 wt % water, 20% AP mixture with the PEGDA (700)/acrylamide mixing ratio of 0.625 wt %. For the hydrogels initiated by TPO and I2959, 5 wt % TPO or I2929 was added into the solution. The hydrogel samples with 140 μm thickness were cured by near UV light with 405 nm wavelength and 25.18 mW/cm^2 power for 2 min. For the hydrogel sample initiated by APS-TEMED, 0.5 wt % APS and 0.05 wt % TEMED were added into the hydrogel solution, and the sample was cured at room temperature for 2 min. The FTIR tests were conducted on an FTIR spectrometer (Bruker, Germany) in conjunction with the single-reflection attenuated total reflectance accessory (64 scans with resolution at 4 cm^{-1}).

To compare the photopolymerization kinetics of the hydrogels initiated by TPO and I2959 (Fig. 3B), we prepared the hydrogel samples by using the abovementioned protocol but UV curing the aqueous solutions with a fix thickness of 140 μm under the near UV light (405 nm) for given time intervals from 5 s to 2 min.

Uniaxial tensile/compressive tests

All the uniaxial tensile/compressive tests were conducted on an MTS uniaxial testing machine (Criterion model 43, MN, USA). For the comparison of the stretch-stress behavior between the AP hydrogels initiated by TPO and APS-TEMED (Fig. 3C), we prepared the hydrogel samples consisting of 80 wt % water and 20% AP mixture with the PEGDA (700)/acrylamide mixing ratio of 1.25 wt %. For the bonding demonstrations and tests (Fig. 3, D to Q), we prepared the hydrogel consisting of 80 wt % water and 20% AP mixture with the PEGDA (700)/acrylamide mixing ratio of 0.625 wt %. For the uniaxial tensile test of the horseshoe structure–reinforced hydrogel composite (Fig. 4B), we printed the matrix with the hydrogel consisting of 80 wt % water and 20% AP mixture with the PEGDA (700)/acrylamide mixing ratio of 0.625 wt % and printed the horseshoe structure with VeroBlack from Stratasys Ltd. (Eden Prairie, MN, USA). For the uniaxial compressive tests for the lattice-reinforced hydrogel cubes (Fig. 4, D to F), we printed the matrix with the hydrogel with the same recipe as the one used above and printed the lattice structures with VeroClear from Stratasys Ltd. (Eden Prairie, MN, USA) added with 0.05% Sudan I (Sigma-Aldrich) to improve the printing resolution. The same solutions were used to print lattice-reinforced meniscus (Fig. 4, G to K).

Thermomechanical behavior of modified VeroClear

We modified the commercial UV curable SMP VeroClear by adding a commercial UV curable monomer epoxy aliphatic acrylate (EAA; Ebecryl 113, Allnex). The mixing ratio between VeroClear and EAA is 8:2. We conducted the dynamic mechanical analysis (DMA) on a DMA machine (TA Q800) to identify the glass transition T_g of the modified VeroClear. The test frequency is 1 Hz, and the temperature was scanned from 100° to 0°C at a cooling rate of −2°C/min. Figure 5E plots the storage modulus and tanδ versus temperature. The T_g was identified at the peak of tanδ that is 30°C. We further performed the shape memory cyclic test. The details are presented in note S9 and fig. S9.

Finite element analysis

To predict the strain on the SPA, FEA simulations were conducted by using the commercially available software package ABAQUS (V6.14, Dassault Systèmes Simulia Corp., USA). We use the third-order hyperelastic Yeoh model with strain energy form $U = \sum_{i=1}^{3} C_i (I_1 - 3)^i$ to describe the nonlinear material behavior of the elastomer. After fitting the uniaxial tensile experiments, the material coefficients were obtained as C_1 = 0.13 MPa, $C_2 = 2.06 \cdot \times 10^{-3}$ MPa, and $C_3 = 2.25 \cdot \times 10^{-3}$ MPa. A half 3D model of the soft actuator was constructed and analyzed on ABAQUS/Standard (Simulia, Dassault Systemes). The pressure was applied to all the internal walls. Solid tetrahedron linear hybrid element (element type C3D4H) was used to mesh the parts. We loaded different pressure in finite element method model to achieve the corresponding bending angles.

SUPPLEMENTARY MATERIALS

Supplementary material for this article is available at http://advances.sciencemag.org/cgi/content/full/7/2/eaba4261/DC1

REFERENCES AND NOTES

1. M. L. Gou, X. Qu, W. Zhu, M. Xiang, J. Yang, K. Zhang, Y. Wei, S. Chen, Bio-inspired detoxification using 3D-printed hydrogel nanocomposites. *Nat. Commun.* **5**, 3774 (2014).
2. B. Grigoryan, S. J. Paulsen, D. C. Corbett, D. W. Sazer, C. L. Fortin, A. J. Zaita, P. T. Greenfield, N. J. Calafat, J. P. Gounley, A. H. Ta, F. Johansson, A. Randles, J. E. Rosenkrantz, J. D. Louis-Rosenberg, P. A. Galie, K. R. Stevens, J. S. Miller, Multivascular networks and functional intravascular topologies within biocompatible hydrogels. *Science* **364**, 458–464 (2019).
3. A. Lee, A. R. Hudson, D. J. Shiwarski, J. W. Tashman, T. J. Hinton, S. Yerneni, J. M. Bliley, P. G. Campbell, A. W. Feinberg, 3D bioprinting of collagen to rebuild components of the human heart. *Science* **365**, 482–487 (2019).
4. C. Keplinger, J.-Y. Sun, C. C. Foo, P. Rothemund, G. M. Whitesides, Z. Suo, Stretchable, transparent, ionic conductors. *Science* **341**, 984–987 (2013).
5. C.-C. Kim, H.-H. Lee, K. H. Oh, J.-Y. Sun, Highly stretchable, transparent ionic touch panel. *Science* **353**, 682–687 (2016).
6. X. Ma, X. Qu, W. Zhu, Y.-S. Li, S. Yuan, H. Zhang, J. Liu, P. Wang, C. S. E. Lai, F. Zanella, G.-S. Feng, F. Sheikh, S. Chien, S. Chen, Deterministically patterned biomimetic human iPSC-derived hepatic model via rapid 3D bioprinting. *Proc. Natl. Acad. Sci. U.S.A.* **113**, 2206–2211 (2016).
7. Y. Takashima, S. Hatanaka, M. Otsubo, M. Nakahata, T. Kakuta, A. Hashidzume, H. Yamaguchi, A. Harada, Expansion-contraction of photoresponsive artificial muscle regulated by host-guest interactions. *Nat. Commun.* **3**, 1270 (2012).
8. Y. Yu, H. Yuk, G. A. Parada, Y. Wu, X. Liu, C. S. Nabzdyk, K. Youcef-Toumi, J. Zang, X. Zhao, Multifunctional "hydrogel skins" on diverse polymers with arbitrary shapes. *Adv. Mater.* **31**, 1807101 (2019).
9. G. A. Parada, H. Yuk, X. Liu, A. J. Hsieh, X. Zhao, Impermeable robust hydrogels via hybrid lamination. *Adv. Healthc. Mater.* **6**, 1700520 (2017).
10. Y. Kim, G. A. Parada, S. Liu, X. Zhao, Ferromagnetic soft continuum robots. *Sci. Robot* **4**, eaax7329 (2019).
11. H. Yuk, T. Zhang, G. A. Parada, X. Liu, X. Zhao, Skin-inspired hydrogel-elastomer hybrids with robust interfaces and functional microstructures. *Nat. Commun.* **7**, 12028 (2016).
12. Q. Liu, G. Nian, C. Yang, S. Qu, Z. Suo, Bonding dissimilar polymer networks in various manufacturing processes. *Nat. Commun.* **9**, 846 (2018).
13. S. Lin, C. Cao, Q. Wang, M. Gonzalez, J. E. Dolbow, X. Zhao, Design of stiff, tough and stretchy hydrogel composites via nanoscale hybrid crosslinking and macroscale fiber reinforcement. *Soft Matter* **10**, 7519–7527 (2014).

14. Y. Huang, D. R. King, T. L. Sun, T. Nonoyama, T. Kurokawa, T. Nakajima, J. P. Gong, Energy-dissipative matrices enable synergistic toughening in fiber reinforced soft composites. *Adv. Funct. Mater.* **27**, 1605350 (2017).
15. X. Liu, T.-C. Tang, E. Tham, H. Yuk, S. Lin, T. K. Lu, X. Zhao, Stretchable living materials and devices with hydrogel-elastomer hybrids hosting programmed cells. *Proc. Natl. Acad. Sci. U.S.A.* **114**, 2200–2205 (2017).
16. S. Lin, H. Yuk, T. Zhang, G. A. Parada, H. Koo, C. Yu, X. Zhao, Stretchable hydrogel electronics and devices. *Adv. Mater.* **28**, 4497–4505 (2016).
17. H. Yuk, S. T. Lin, C. Ma, M. Takaffoli, N. X. Fang, X. Zhao, Hydraulic hydrogel actuators and robots optically and sonically camouflaged in water. *Nat. Commun.* **8**, 14230 (2017).
18. S. Hong, D. Sycks, H. F. Chan, S. Lin, G. P. Lopez, F. Guilak, K. W. Leong, X. Zhao, 3D printing of highly stretchable and tough hydrogels into complex, cellularized structures, cellularized structures. *Adv. Mat.* **27**, 4035–4040 (2015).
19. A. S. Gladman, E. A. Matsumoto, R. G. Nuzzo, L. Mahadevan, J. A. Lewis, Biomimetic 4D printing. *Nat. Mater.* **15**, 413–418 (2016).
20. H. Yuk, X. Zhao, A new 3D printing strategy by harnessing deformation, instability, and fracture of viscoelastic inks. *Adv. Mat.* **30**, 1704028 (2018).
21. K. Tian, J. Bae, S. E. Bakarich, C. Yang, R. D. Gately, G. M. Spinks, M. in het Panhuis, Z. Suo, J. J. Vlassak, 3D printing of transparent and conductive heterogeneous hydrogel-elastomer systems. *Adv. Mat.* **29**, 1604827 (2017).
22. M. A. Skylar-Scott, J. Mueller, C. W. Visser, J. A. Lewis, Voxelated soft matter via multimaterial multinozzle 3D printing. *Nature* **575**, 330–335 (2019).
23. C. Yuan, K. Kowsari, S. Panjwani, Z. Chen, D. Wang, B. Zhang, C. J.-X. Ng, P. V. Y. Alvarado, Q. Ge, Ultrafast three-dimensional printing of optically smooth microlens arrays by oscillation-assisted digital light processing. *ACS Appl. Mater. Interfaces* **11**, 40662–40668 (2019).
24. K. Kowsari, S. Akbari, D. Wang, N. X. Fang, Q. Ge, High-efficiency high-resolution multimaterial fabrication for digital light processing-based three-dimensional printing. *3D Print. Addit. Manuf.* **5**, 185–193 (2018).
25. Y.-F. Zhang, C. J.-X. Ng, Z. Chen, W. Zhang, S. Panjwani, K. Kowsari, H. Y. Yang, Q. Ge, Miniature pneumatic actuators for soft robots by high-resolution multimaterial 3D printing. *Adv. Mat. Technol.* **4**, 1900427 (2019).
26. X. Zheng, W. Smith, J. Jackson, B. Moran, H. Cui, D. Chen, J. Ye, N. Fang, N. Rodriguez, T. Weisgraber, C. M. Spadaccini, Multiscale metallic metamaterials. *Nat. Mater.* **15**, 1100–1106 (2016).
27. B. Zhang, S. Li, H. Hingorani, A. Serjouei, L. Larush, A. A. Pawar, W. H. Goh, A. H. Sakhaei, M. Hashimoto, K. Kowsari, S. Magdassi, Q. Ge, Highly stretchable hydrogels for UV curing based high-resolution multimaterial 3D printing. *J. Mater. Chem. B* **6**, 3246–3253 (2018).
28. A. A. Pawar, G. Saada, I. Cooperstein, L. Larush, J. A. Jackman, S. R. Tabaei, N.-J. Cho, S. Magdassi, High-performance 3D printing of hydrogels by water-dispersible photoinitiator nanoparticles. *Sci. Adv.* **2**, e1501381 (2016).
29. V. Chan, P. Zorlutuna, J. H. Jeong, H. Kong, R. Bashir, Three-dimensional photopatterning of hydrogels using stereolithography for long-term cell encapsulation. *Lab Chip* **10**, 2062–2070 (2010).
30. V. Chan, J. H. Jeong, P. Bajaj, M. Collens, T. Saif, H. Kong, R. Bashir, Multi-material bio-fabrication of hydrogel cantilevers and actuators with stereolithography. *Lab Chip* **12**, 88–98 (2012).
31. D. Han, Z. Lu, S. A. Chester, H. Lee, Micro 3D printing of a temperature-responsive hydrogel using projection micro-stereolithography. *Sci. Rep.* **8**, 1963 (2018).
32. D. Han, C. Farino, C. Yang, T. Scott, D. Browe, W. Choi, J. W. Freeman, H. Lee, Soft robotic manipulation and locomotion with a 3D printed electroactive hydrogel. *ACS Appl. Mater. Interfaces* **10**, 17512–17518 (2018).
33. J.-Y. Sun, X. Zhao, W. R. K. Illeperuma, O. Chaudhuri, K. H. Oh, D. J. Mooney, J. J. Vlassak, Z. Suo, Highly stretchable and tough hydrogels. *Nature* **489**, 133–136 (2012).
34. D. K. Patel, A. H. Sakhaei, M. Layani, B. Zhang, Q. Ge, S. Magdassi, Highly stretchable and UV curable elastomers for digital light processing based 3D printing. *Adv. Mater.* **29**, 1606000 (2017).
35. Q. Ge, A. H. Sakhaei, H. Lee, C. K. Dunn, N. X. Fang, M. L. Dunn, Multimaterial 4D printing with tailorable shape memory polymers. *Sci. Rep.* **6**, 31110 (2016).
36. S. E. Bakarich, R. Gorkin, M. in het Panhuis, G. M. Spinks, Three-dimensional printing fiber reinforced hydrogel composites. *ACS Appl. Mater. Interfaces* **6**, 15998–16006 (2014).
37. S. E. Bakarich, R. Gorkin, R. Gately, S. Naficy, M. in het Panhuis, G. M. Spinks, 3D printing of tough hydrogel composites with spatially varying materials properties. *Addit. Manuf.* **14**, 24–30 (2017).
38. J. Visser, F. P. W. Melchels, J. E. Jeon, E. M. van Bussel, L. S. Kimpton, H. M. Byrne, W. J. A. Dhert, P. D. Dalton, D. W. Hutmacher, J. Malda, Reinforcement of hydrogels using three-dimensionally printed microfibres. *Nat. Commun.* **6**, 6933 (2015).
39. Q. Ma, H. Cheng, K.-I. Jang, H. Luan, K.-C. Hwang, J. A. Rogers, Y. Huang, Y. Zhang, A nonlinear mechanics model of bio-inspired hierarchical lattice materials consisting of horseshoe microstructures. *J. Mech. Phys. Solids* **90**, 179–202 (2016).
40. D. Wang, Y. Xiong, B. Zhang, Y.-F. Zhang, D. Rosen, Q. Ge, Design framework for mechanically tunable soft biomaterial composites enhanced by modified horseshoe lattice structures. *Soft Matter* **16**, 1473–1484 (2020).
41. J. A. Fan, W.-H. Yeo, Y. Su, Y. Hattori, W. Lee, S.-Y. Jung, Y. Zhang, Z. Liu, H. Cheng, L. Falgout, M. Bajema, T. Coleman, D. Gregoire, R. J. Larsen, Y. Huang, J. A. Rogers, Fractal design concepts for stretchable electronics. *Nat. Commun.* **5**, 3266 (2014).
42. J. Li, D. J. Mooney, Designing hydrogels for controlled drug delivery. *Nat. Rev. Mater.* **1**, 16071 (2016).
43. A. N. Steele, L. M. Stapleton, J. M. Farry, H. J. Lucian, M. J. Paulsen, A. Eskandari, C. E. Hironaka, A. D. Thakore, H. Wang, A. C. Yu, D. Chan, E. A. Appel, Y. J. Woo, A biocompatible therapeutic catheter-deliverable hydrogel for in situ tissue engineering. *Adv. Healthc. Mater.* **8**, 1801147 (2019).
44. P. Gupta, K. Vermani, S. Garg, Hydrogels: From controlled release to pH-responsive drug delivery. *Drug Discov. Today* **7**, 569–579 (2002).
45. K. Elgeneidy, G. Neumann, M. Jackson, N. Lohse, Directly printable flexible strain sensors for bending and contact feedback of soft actuators. *Front. Robot. AI* **5**, 2 (2018).
46. S. Cheng, Y. S. Narang, C. Yang, Z. Suo, R. D. Howe, Stick-on large-strain sensors for soft robots. *Adv. Mater. Interfaces* **6**, 1900985 (2019).
47. J. C. Yeo, H. K. Yap, W. Xi, Z. Wang, C.-H. Yeow, C. T. Lim, Flexible and stretchable strain sensing actuator for wearable soft robotic applications. *Adv. Mater. Technol.* **1**, 1600018 (2016).
48. T. Pinto, L. Cai, C. Wang, X. Tan, CNT-based sensor arrays for local strain measurements in soft pneumatic actuators. *Int. J. Intell. Robot. Appl.* **1**, 157–166 (2017).
49. S.-Z. Guo, K. Qiu, F. Meng, S. H. Park, M. C. McAlpine, 3D printed stretchable tactile sensors. *Adv. Mater.* **29**, 1701218 (2017).
50. J. T. Muth, D. M. Vogt, R. L. Truby, Y. Mengüç, D. B. Kolesky, R. J. Wood, J. A. Lewis, Embedded 3D printing of strain sensors within highly stretchable elastomers. *Adv. Mater.* **26**, 6307–6312 (2014).

Acknowledgments

Funding: Q.G. acknowledges the Key-Area Research and Development Program of Guangdong Province (no. 2020B090923003). Z.C. and S.Q. acknowledge the National Natural Science Foundation of China (nos. 11525210 and 91748209) and the Fundamental Research Funds for the Central Universities (no. 2020XZZX005-02). B.Z. acknowledges the Fundamental Research Funds for the Central Universities (no. 31020190QD015) and the National Natural Science Foundation of China (no. 51903210). H.L. acknowledges the support provided by China Scholarship Council (CSC) for study at SUTD (CSC201806130090). **Author contributions:** Q.G., Z.C., B.Z., and S.Q. conceived the ideas and designed the research. Z.C., J.C., B.Z., Y.-F.Z., H.L., X.H., and C.Y. carried out the experiments. X.H. and S.M. contributed to the approach of developing water-soluble TPO. Q.G. drafted the manuscript. Q.G., Z.C., B.Z., J.L., and S.Q. contributed to the writing of the manuscript. **Competing interests:** The authors declare that they have no competing interests. **Data and materials availability:** All data needed to evaluate the conclusions in the paper are present in the paper and/or the Supplementary Materials. Additional data related to this paper may be requested from the authors.

Submitted 3 December 2019
Accepted 10 November 2020
Published 6 January 2021
10.1126/sciadv.aba4261

Citation: Q. Ge, Z. Chen, J. Cheng, B. Zhang, Y.-F. Zhang, H. Li, X. He, C. Yuan, J. Liu, S. Magdassi, S. Qu, 3D printing of highly stretchable hydrogel with diverse UV curable polymers. *Sci. Adv.* **7**, eaba4261 (2021).